Viscosuperelasticity: A comprehensive interpretation of non-reciprocal isothermal dynamics, kinetic arrest, and non-ergodic anelastic strain based on thermal activation of martensitic transformations

K. Niitsu[a,b]*, Y. Yano[b], R. Kainuma[c], H. Inui[b,d]

[a] National Institute for Materials Science, Tsukuba 305-0047, Japan

[b] Department of Materials Science and Engineering, Kyoto University, Kyoto 606-8501, Japan

[c] Department of Materials Science, Graduate School of Engineering, Tohoku University, Sendai 980-8579, Japan

[d] Center for Elements Strategy Initiative for Structure Materials (ESISM), Kyoto University, Kyoto 606-8501, Japan

*Corresponding author. Tel.: +81-29-859-2566; e-mail: NIITSU.Kodai@nims.go.jp

ABSTRACT

Much of the impact of thermal activation on the low-temperature dynamics of the thermoelastic martensitic transformation (MT) remains unresolved. This study introduces a new concept of "viscosuperelasticity" to comprehensively interpret the slow dynamics of stress-induced MT at low temperatures. The thermal activation dynamics underlying this concept allow for deriving the *time-temperature-transformation* (*TTT*) diagrams at any holding stress from the temperature- and strain-rate-dependent superelastic stress-strain curves. Experimental results for isothermal forward and reverse MTs comprehensively agree with the derived *TTT* diagrams, disclosing the non-reciprocity in the dynamics between the forward and reverse MT paths. One of the representative manifestations of "viscosuperelasticity" is the difference in the cooling/heating rate dependence of the forward/reverse MT starting and finishing temperatures (T_{Ms}, T_{Mf}, T_{As}, and T_{Af}). A significant decrease in T_{Ms} and T_{Mf} with increasing cooling rate explains kinetic arrest, and a gradual increase in T_{As} and T_{Af} with increasing heating rate explains the difficulty in detecting the isothermal evolution of the reverse MT. The *TTT* diagrams also enable the impact of thermal activation upon dynamic cooling/heating to be evaluated quantitatively, explaining the non-ergodic thermal-history dependence of anelastic transformation strain, which is believed to be an essential signature of strain glass. The concept of "viscosuperelasticity" offers a comprehensive interpretation of non-reciprocal isothermal dynamics, kinetic arrest, and non-ergodicity in the anelastic strain as manifestations of thermal activation of MTs.

Keywords: Thermally activated process; Martensitic transformation; Kinetics; Shape memory alloys; Isothermal martensitic transformation

1. INTRODUCTION

Since the discovery of the isothermal martensitic transformation (MT) in Fe-Mn-C [1] and Fe-Ni-Mn alloys [2], numerous studies have fostered a consensus that MT dynamics have both athermal and thermal nature [3–6]. Athermal dynamics, which depend on intensive variables such as temperature, stresses, magnetic fields, and chemical potential, essentially exist in any first-order phase transformation and give rise to finite transformation hysteresis for driving transforming interfaces. In contrast, isothermal (thermally activated) dynamics depend on time along with the aforementioned intensive variables and are more pronounced at low temperatures where thermal excitations are stochastically suppressed [7]. These two natures should be independently considered for nucleation and growth, the processes by which MTs develop. Earlier studies on thermally-induced MTs have concluded that the rate-controlling process is martensite nucleation (followed by auto-catalytic ultrafast growth) rather than growth [3–5]. This conclusion seems reasonable because, in the case of thermally-induced MTs, a large part of the excess energy could be consumed to overcome the nucleation barrier, and once nucleation occurs, the nuclei instantaneously grow into martensite variants. A similar scenario could be the case for magnetic-field-induced MTs [8].

Meanwhile, a detailed study on the kinetics of thermally-induced MT in a Cu-Zn-Al alloy revealed that the MT process is governed by continuous growth, with only 5% involving jerks which may be responsible for nucleation [9]. Furthermore, unlike thermally- and magnetic-field-induced MTs, stress-induced MTs should be primarily

governed by the growth process because a reduced number of variants with higher resolved shear stresses is preferred for activation. Macroscopically smooth propagation of the interface (habit plane) is observed during the evolution of stress-induced MTs. As a result, the nucleation process is typically not manifested in superelastic stress-strain curves [10].

The earlier conclusion was drawn on nucleation, thus is inadequate to interpret stress-induced MTs that proceed predominantly by growth. Following a study by Ghosh and Raghavan, which reported the effect of superimposed stresses [11], they stated that isothermal MT could significantly develop even under stress. They discussed this within the framework of earlier models based on martensite nucleation [3,12–16]. This conceptualization has led to the classification of "athermal" and "isothermal" dynamics as being promoted by long-range stress fields and by short-range interactions of point defects, respectively, which enlightens the phenomenological similarity to the dynamics of slip deformation [17,18]. Keeping this in mind, Kajiwara claimed the microscopic role of dislocations on the dynamics of isothermal MTs [19–21], according to which the generation of dislocations leading to the formation of martensite is a rate-controlling process. Since the thermally activated dislocation motion underlying these two events governs the isothermal MT dynamics, the possibility of isothermal macroscopic growth (which may be microscopically constituted by avalanches [22]) of the martensite variants, which was not considered earlier, can not be ruled out. Furthermore, this hypothesis suggests the possibility of an isothermal "reverse" MT driven by habit plane propagation

rather than nucleation. As demonstrated later, this study clarifies that the isothermal reverse MT indeed occurs, enlightening the predominant role of the reversible growth process in isothermal MTs.

The most representative feature of the isothermal forward MT is the presence of a C-shaped contour curve in the *time–temperature–transformation* (*TTT*) diagram [6]. Some models based on the thermal excitation of martensite nuclei have been proposed to explain this behavior [23–25]. Although these models reproduce a C-shaped contour curve for the isothermal forward MT, there remains a concern that the underlying assumption of the models may be applicable to only a limited aspect of the overall MT evolution. More specifically, the homogeneous nucleation assumed in some models may not be suitable for real systems as nucleation is highly inhomogeneous. Besides, the models were proposed for nucleation and did not assume isothermal growth, which could constitute a large portion of the MT evolution. In this sense, the growth-driven reverse MT is out of the scope of existing models. More importantly, no model currently includes prerequisites to account for non-reciprocity in the isothermal forward and reverse MT paths. The existing models are not applicable to the reverse MT, or even if possible, the predicted reverse dynamics would be exactly reciprocal to the forward one, calling into question the implication of "nucleation".

In addition to isothermal dynamics, the possible impact of thermal activation on the MT dynamics under the dynamic sweep of external fields is of practical interest because the MT-starting/finishing temperatures, stresses, and magnetic fields, are usually

determined under the sweep of corresponding fields. Isothermal dynamics should be superimposed even during the dynamic sweep, but its impact has not yet been clarified.

As mentioned above, interpreting the overall dynamics of MTs is not straightforward. Various theoretical or phenomenological models have been proposed, but they can only shape limited aspects. To resolve this disruption, a comprehensive picture encompassing the phenomenology of MT dynamics, including the athermal/isothermal, nucleation/growth, and forward/reverse concepts, is necessary. The authors consider that the stress-induced MTs provide an appropriate platform for studying growth dynamics, as other cases (thermally- and magnetically-induced MTs) involve both nucleation and growth and thus are likely to be complex to analyze.

Recent studies on the low-temperature behavior of stress-induced MTs have revealed that the temperature and strain-rate dependence of transformation hysteresis becomes more pronounced at lower temperatures (typically below 200 K) for many alloy systems [26–32]. This tendency was interpreted as a manifestation of the thermal activation of habit plane propagation. For modeling this tendency, a mathematical description that mimics the thermally-activated dynamics of dislocation glides was proposed [18,31,33–35] (see ref. [31] for a detailed explanation of this equation):

$$\sigma_{eff}\left(\approx\frac{\sigma_{hys}}{2}\right)=\sigma_{\mu}+\sigma_{TA}\left[1-\left\{\frac{k_BT}{Q}\ln\left(\frac{\dot{\varepsilon}_0}{\dot{\varepsilon}_{SE}}\right)\right\}^{1/q}\right]^{1/p} \quad (1)$$

where σ_{μ} and σ_{TA} represent the athermal component and thermal activation offset at 0 K for the overloading/underloading stresses required to drive the forward/reverse MTs, respectively; Q the activation energy at 0 K; k_B the Boltzmann constant; $\dot{\varepsilon}_0$ a pre-

exponential factor; $\dot{\varepsilon}_{SE}$ the superelastic strain rate; and p and q are fitting parameters that characterize the curvature of the temperature and strain-rate dependence of σ_{eff}. It is empirically known that the combination of $p = 1/2$ and $q = 3/2$ is the most reproducible. According to the original Seeger's formulation, this combination shapes the Peierls potential by misfit stresses [33]. Equation 1 indicates that the effective stress (σ_{eff}) required to drive the habit planes, usually approximated as half of the transformation hysteresis (σ_{hys}), can be decomposed into two components of an athermal term and a thermal activation term. Accordingly, if the proposed form can explicitly depict the impact of thermal activation on growth, the isothermal dynamics could also be comprehended with an extension of this form, as the strain rate involves the dimension of time.

In this study, this idea was verified by examining its applicability to both the isothermal forward and reverse MTs. This examination was demonstrated for a prototypical Ni-rich Ti-Ni superelastic alloy, which is known to exhibit a remarkable dependence of transformation stress hysteresis on temperature and strain rate [28,31]. In addition to modeling the macroscopic responses, the isothermal growth of the martensite variants was directly observed by *in situ* transmission electron microscopy (TEM) under uniaxial tensile stress. The impact of thermal activation on the MT behaviors under the dynamic cooling/heating was quantitatively evaluated based on the isothermal nature. The possible origin of kinetic arrest and non-ergodic behavior of anelastic transformation strains, which is often regarded as a signature of strain glass [36,37], is discussed in terms

of the underlying thermal activation nature. While it has been previously considered that these phenomena have different origins, it is found that they are commonly related to the slow dynamics of MTs governed by thermal activation. To provide a comprehensive interpretation of these phenomena, a new concept of "viscosuperelasticity" is introduced following the concept of viscoplasticity.

2. EXPERIMENTAL

A Ti-51.8Ni (at.%) alloy was fabricated using arc melting. At this composition, the thermally-induced MT is completely suppressed without the help of stress [26]. The obtained polycrystalline button was homogenized at 1173 K for 24 h, followed by quenching in water. A 3.5 × 3.5 × 10.5 mm specimen was cut from the button for compression testing. The temperature dependence of the compressive stress-strain curves at 30–220 K was examined. Isothermal stress relaxations were examined at 82 K, and isothermal strain evolutions (isothermal MTs) were recorded at various temperatures under holding compressive stresses (σ_h) of 500 and 200 MPa for the forward and reverse MT paths, respectively. The isothermal reverse MT was recorded by interrupting the unloading sequence at 200 MPa after reversing the forward stressing sequence at a superelastic strain (ε_{SE}) of 0.0450, which is approximately 82% of the full superelastic strain (ε_{full}) (= 0.0550). The temperature oscillation during isothermal holding was within ±2 K. All mechanical tests were performed on one specimen, and the total number of tests was < 50, within which cyclic fatigue is insignificant [22]. It was also confirmed that the

strain relaxation for 1×10^6 s of the specimen and compression jigs under isothermal holding at 10 K and σ_h = 300 MPa was less than 0.0007. *In situ* TEM observations were conducted at 95 and 220 K under uniaxial tensile stress using a combination of a TEM and a single-tilt liquid nitrogen cooling straining holder [38]. The observation area was thinned by electrochemical polishing in a solution of 72% acetic acid, 12% ethanol, 8% ethylene glycol, and 8% perchloric acid.

3. RESULTS

3.1. DYNAMIC PHASE DIAGRAM

Figure 1a shows the temperature dependence of the superelastic behavior. As previously reported for this alloy system [26,30,31], the transformation hysteresis increases significantly with decreasing temperature. This is a typical manifestation of the thermal activation of stress-induced MTs [26]. The equilibrium stress (σ_0) is typically approximated as the midpoint between the forward/reverse MT starting/finishing stresses (σ_M and σ_A) [39]. The temperature dependence of σ_0 was drawn to follow the Clausius-Clapeyron relationship wherein the transformation entropy change obeys the third law of thermodynamics [40]. The effective overloading/underloading stress required to drive the forward/reverse MTs, σ_{eff}, is shown in Fig. 1c as a function of temperature. The curve fitted using Eq. 1 was in close agreement with the experimental plots (Fig. 1b and c; numerical values of the parameters are given in the caption). Equation 1 can be converted to the Arrhenius form:

$$\ln \dot{\varepsilon}_{SE} = \ln \dot{\varepsilon}_0 - \frac{Q}{k_B T}\left[1 - \left(\frac{\sigma_{eff} - \sigma_\mu}{\sigma_{TA}}\right)^p\right]^q \equiv \ln \dot{\varepsilon}_0 - QZ(T, \dot{\varepsilon}_{SE}), \qquad (2)$$

which enables the evaluation of Q and $\dot{\varepsilon}_0$ from the gradient and intercept of the fitting line, respectively (see inset of Fig. 1c).

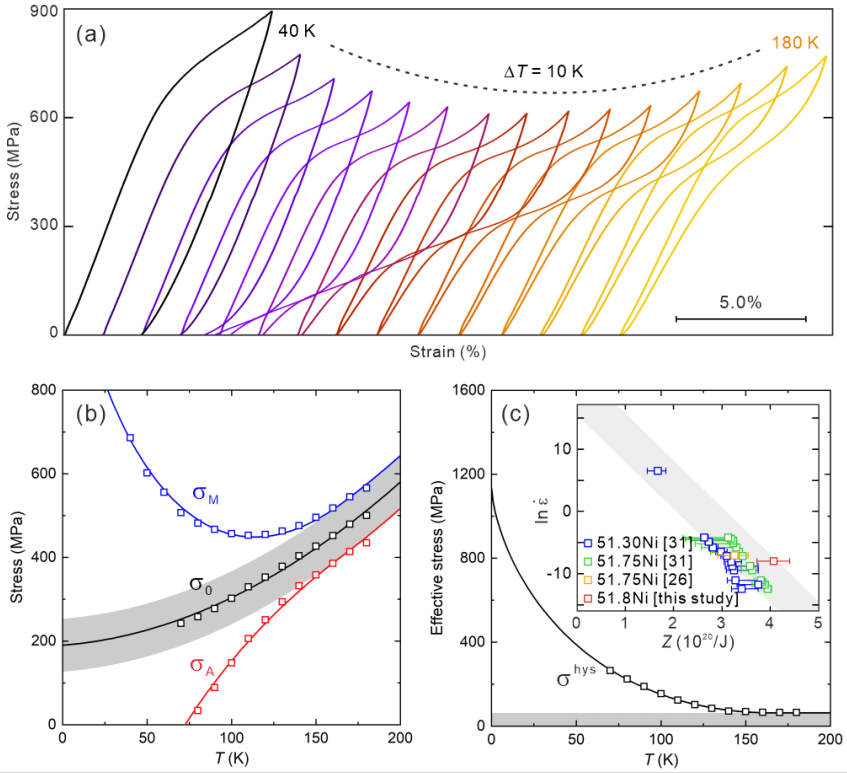

Fig. 1. Temperature dependence of (a) the superelastic stress-strain curves, (b) σ_M, σ_A, and σ_0, and (c) σ_{eff}. Inset in (c) represents the Arrhenius plot of Eq. 2. The tests were carried out at a constant strain rate of 3.3×10^{-4} s^{-1}. The numerical values of the parameters in Eq. 1 were as follows: σ_μ = 63 MPa, σ_{TA} = 1073 MPa, Q = 0.47 eV, $\dot{\varepsilon}_0$ = 8.0×10^8 s^{-1} (with an error of 2.7×10^7–5.9×10^{10}), p = 1/2, and q = 3/2.

As Eq. 1 implicitly includes the dimension of time in $\dot{\varepsilon}_{SE}$, this contribution is made explicit. In the simple framework of viscoplasticity [41], the strain rate is decomposed into the parts of elasticity (ε_e) and viscoplasticity (ε_{vp}), that is, $\dot{\varepsilon} = \frac{\partial \varepsilon_e}{\partial t} + \frac{\partial \varepsilon_{vp}}{\partial t}$. The former part is given by $\frac{\partial \varepsilon_e}{\partial t} = \frac{1}{E_A}\frac{\partial \sigma}{\partial t}$ referring to Hooke's law, with the elastic modulus of the austenite phase (E_A). Considering the stress relaxation condition,

the total strain rate $\dot{\varepsilon}$ is zero. Hence we have $\frac{\partial \varepsilon_{vp}}{\partial t} = -\frac{1}{E_A}\frac{\partial \sigma}{\partial t}$. As mentioned, Eq. 1 is derived by mimicking Seeger's formulation for thermal activation of dislocation glides. It is thus a generic scheme that ε_{vp} corresponds to ε_{SE} in the context of "viscosuperelasticity" and that the stress component exhibiting temperature and time dependence is $\sigma_{eff} - \sigma_{\mu}$. Therefore, for the stress relaxation condition, Eq. 2 can be converted to

$$\frac{\partial\left(\sigma_{eff} - \sigma_{\mu}\right)}{\partial t} = -E_A \exp\left\{\ln \dot{\varepsilon}_0 - \frac{Q}{k_B T}\left[1 - \left(\frac{\sigma_{eff} - \sigma_{\mu}}{\sigma_{TA}}\right)^p\right]^q\right\}. \quad (3)$$

Here, one might question the applicability of Hooke's law to the superelastic regime. Eq. 3 should be logically valid up to the upper limit of the elastic regime. However, the solution of Eq. 3 remains phenomenologically valid at any stage of the stress-induced MTs; otherwise the transformation hysteresis would change as the MTs progress. Equation 3 is the time differential equation of $\sigma_{eff} - \sigma_{\mu}$ (that is, the thermal activation component of effective stresses). Therefore, the time dependence of σ_{eff} at fixed temperature and strain can be derived by solving this equation; a prototypical solution is shown in Fig. 2a. The significant decrease of σ_{eff} over time is a straightforward consequence of its thermal activation nature. Instead, σ_0 up- or downshifts in response to the transformation hardening as the forward/reverse MTs progress, as schematically illustrated in Fig. 2a. The thick black curve corresponds to the dynamic stress-strain curves showing experimentally accessible superelastic behavior. This figure tells us how the superelastic stress-strain curve is captured under dynamic stressing; the thick black

curve traces the $\sigma_0 + \sigma_{eff}$ surface depending on time as well as V_M, thus exhibiting a strain-rate dependence. This trend is experimentally confirmed by the isothermal stress relaxation tests, as shown in Fig. 2b and c. Despite the change in stress level, the magnitude of stress relaxation was almost unchanged with respect to V_M and followed the relaxation curve derived from Eq. 3. As demonstrated later, the *TTT* diagram is derived for the strain relaxation condition. Under this condition, isothermal forward and reverse MT progresses depending on how far the calculated relaxation stress falls below and exceeds σ_h, respectively.

Figure 2 illustrates the impact of thermal activation on transforming stresses. By incorporating this contribution into the observed phase diagram (Fig. 1b), the so-called dynamic phase diagram can be derived, as shown in Fig. 3. This diagram unveils the substantial yet obscured influence of time on MT dynamics. The experimentally determined phase diagram (Fig. 1b) is now interpreted to represent a specific (but not precisely constant) time section of Fig. 3.

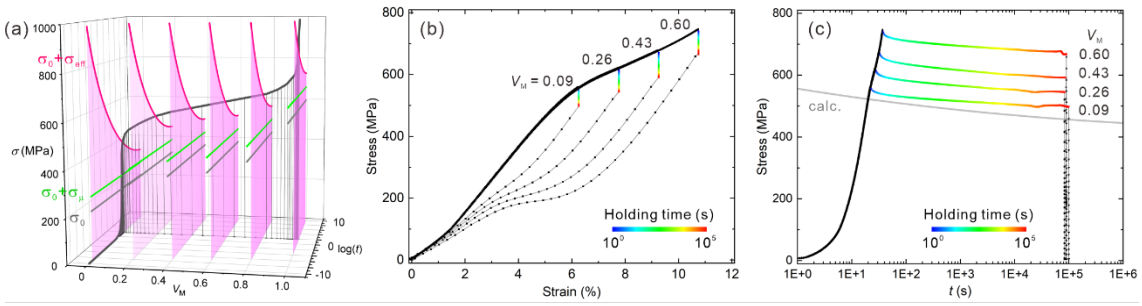

Fig. 2. (a) Typical solution of Eq. 3 for the forward MT at 100 K. The gray, green, and magenta curves represent σ_0, $\sigma_0 + \sigma_\mu$, and $\sigma_0 + \sigma_{eff}$, respectively, drawn for the V_M interval of 0.2. The thick black curve is a schematic drawing of the stress-strain curve observed under dynamic stressing. Superelasticity at 82 K interrupted at several superelastic strains

is shown in the (b) stress-strain and (c) stress-time coordinates. The holding time is overlaid with the inserted color scale. The strain rate to reach the holding strain was 3.3 $\times 10^{-3}$ s^{-1}.

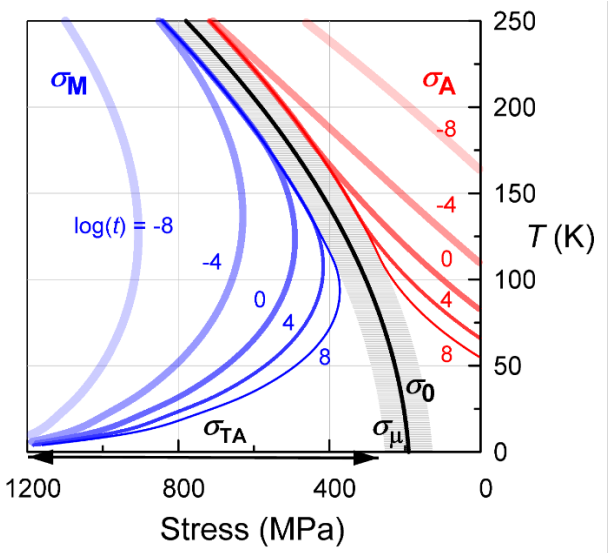

Fig. 3. Dynamic phase diagram as functions of temperature, stress, and time. The blue and red curves are time-dependent σ_M (= σ_0 +σ_{eff}) and σ_A (= σ_0 −σ_{eff}), respectively. σ_{eff} is calculated from Eq. 3.

3.2. ISOTHERMAL TRANSFORMATION DYNAMICS

Figure 3 represents the time dependence of σ_M and σ_A, both of which are originally defined as the endpoint of the elastic deformation regime of the austenite phase (that is, $V_M = 0$). As demonstrated in Fig. 2, however, similar diagrams are derivable for any V_M by simply shifting σ_0. To explicitly visualize the time evolution of MTs, namely, the isothermal transformation dynamics, these convoluted dynamic phase diagrams were cross-sectioned at given σ_h; see Fig. 4a and b for the isothermal forward and reverse MTs, respectively. The derived *TTT* diagrams disclose some critical characteristics of the isothermal transformation dynamics. In the isothermal forward MT, the well-known C-

shaped contour lines are reproduced and are found to be analogous across arbitrary σ_h sections and V_M contours. Additionally, the projection of the nose temperature on the contours (Fig. 4c) shows a non-monotonic variation over time, indicating that the nose temperature is also time-dependent. In contrast, the contour lines of the isothermal reverse MT are characterized by the lower half of the C-shaped curves; hence the nose temperature is missing.

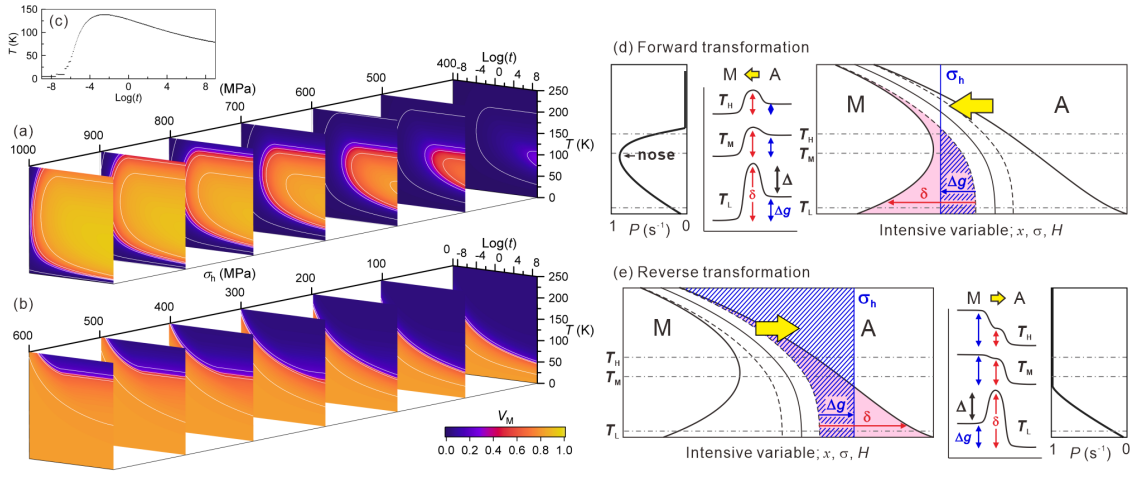

Fig. 4. Stress-sectioned *TTT* diagrams for the isothermal (a) forward and (b) reverse MTs. White contour lines are drawn for the V_M interval of 0.2. (c) Nose temperature for the isothermal forward MT as a function of time. Schematics of the isothermal dynamics for the (d) forward and (e) reverse MTs. Note that Δg and δ in the energy diagrams of (d) and (e) are the thermodynamic and non-thermodynamic (thermally surmountable) energy gaps, respectively, but illustrated in a unique scheme for simplicity.

It is now apparent that the isothermal dynamics of the forward and reverse MTs are not reciprocal. The origin of such non-reciprocal dynamics is outlined in the schematic diagrams of Fig. 4d and e. Considering the forward MT with fixed stress (σ_h) and temperature (T_L, T_M, and T_H) as shown in the right panel of Fig. 4d, the remaining energy barrier Δ (= $\delta - \Delta g$, where δ is the time-dependent thermal activation barrier for driving

MTs and Δg is an offset given by σ_h in the thermal activation regime) that must be overcome by the thermal activation process is very high at a low temperature (T_L), resulting in a considerable stagnation of the isothermal evolution. Δ takes a minimum at an intermediate temperature (T_M), and the isothermal transformation proceeds most easily. The higher temperature becomes, the lower δ is (see $T = T_H$); however, the athermal barrier becomes pronounced as the $\sigma_0 + \sigma_\mu$ curve approaches the σ_h line, again increasing Δ (see the middle panel of Fig. 4d). As illustrated in the left panel of Fig. 4d, the transition probability ($P \propto \Delta^{-1}$) draws a C-shaped curve with a nose temperature at approximately T_M, and the upper-temperature limit of the isothermal forward MT is defined as the intersection of the σ_h line and $\sigma_0 + \sigma_\mu$ curve. In contrast, Δ in the reverse MT (Fig. 4e) decreases monotonically with increasing temperature as Δg increases and δ decreases (see the middle panel of Fig. 4e). This means that P increases with increasing temperature and reaches 1 at the intersection of the σ_h line and $\sigma_0 - \sigma_{eff}$ curve (see the right panel of Fig. 4e), above which the reverse transformation proceeds without incubation; therefore, there is no upper limit on the *TTT* curves for the isothermal reverse MT. The thermodynamic σ_0 curve, which has not been accounted for in any existing kinetic models, plays a critical role in making the isothermal dynamics of the forward and reverse MTs non-reciprocal.

The derived *TTT* diagrams were verified by performing isothermal compression tests at various combinations of σ_h and T, the results of which are presented in the stress-strain diagram in Fig. 5. V_M is also shown in this figure, which was estimated by the mathematical fitting of the superelastic stress-strain curves (refer to Appendix A for the

detailed protocol). Notably, isothermal transformation occurs in both the forward and reverse MT paths. Figure 6 compares the experimental and calculated results. The right panels in Fig. 6a and b show the time evolution of V_M in the isothermal forward and reverse MT paths, respectively; the locations of the monitored segments are overlaid on the corresponding *TTT* diagrams (left panels of Fig. 6a and b). Despite the calculated curves of the forward path showing non-trivial variations with time and temperature, they closely reproduce the overall observed isothermal dynamics. The dynamics are significantly suppressed at lower (such as 32 K) and higher (such as 160 K) temperatures and become more pronounced at intermediate temperatures (such as 100 and 115 K) within the monitored time scale. Similarly, the calculations for the reverse path successfully capture the overall observed trend. Nearly full reverse transformation is observed isothermally at 100 K, dispelling doubts about the existence of the isothermal reverse MT [42]. It should be noted that the small spikes are due to temperature fluctuations and thus are not intrinsic.

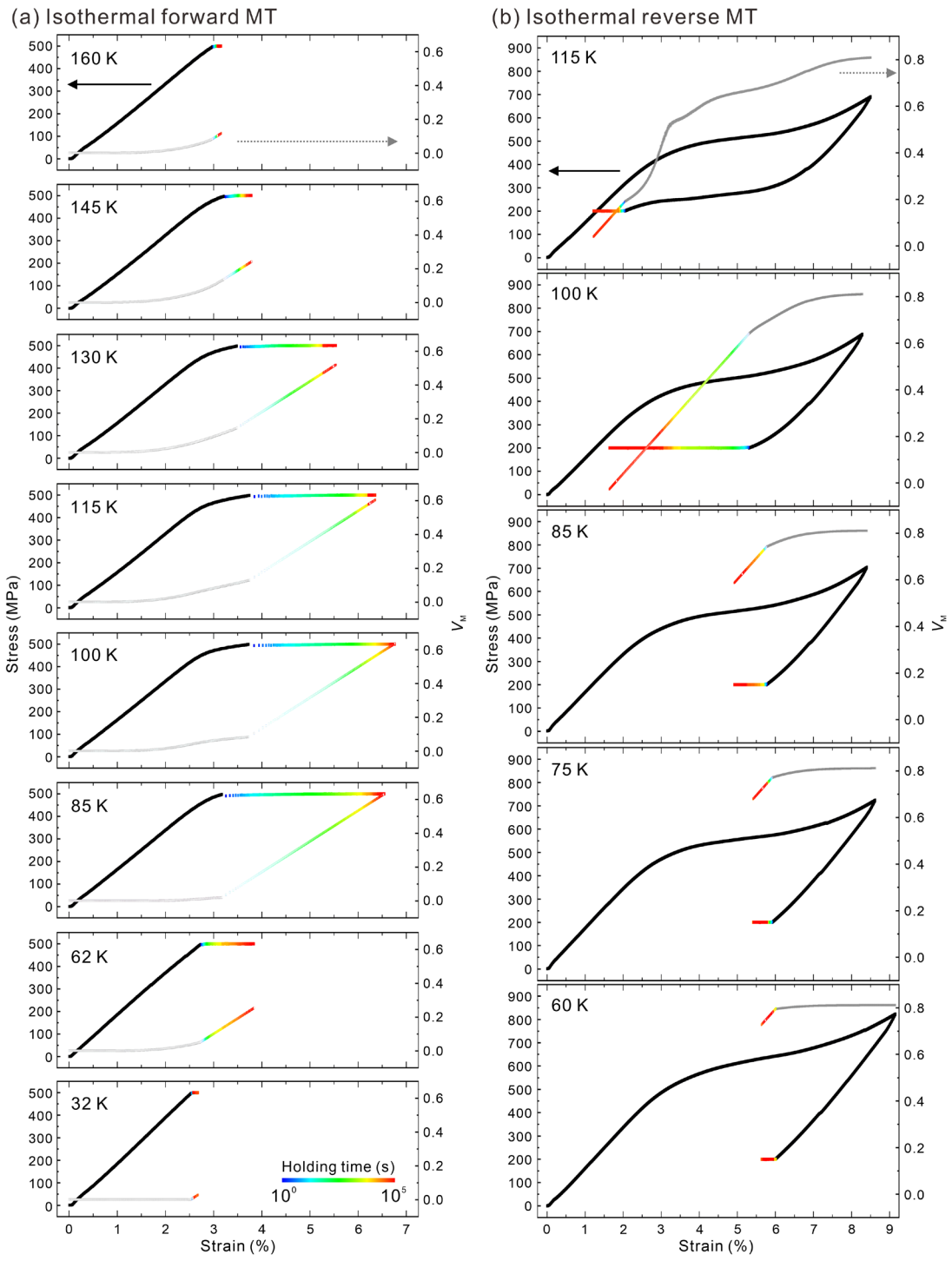

Fig. 5. Isothermal compressive test results for (a) forward path at σ_h = 500 MPa and (b) reverse path at σ_h = 200 MPa. Along with the stress-strain response, V_M is depicted in gray. The holding time at σ_h is overlaid with the inserted color scale. The strain rate to reach the holding stress was 3.3×10^{-3} s^{-1}.

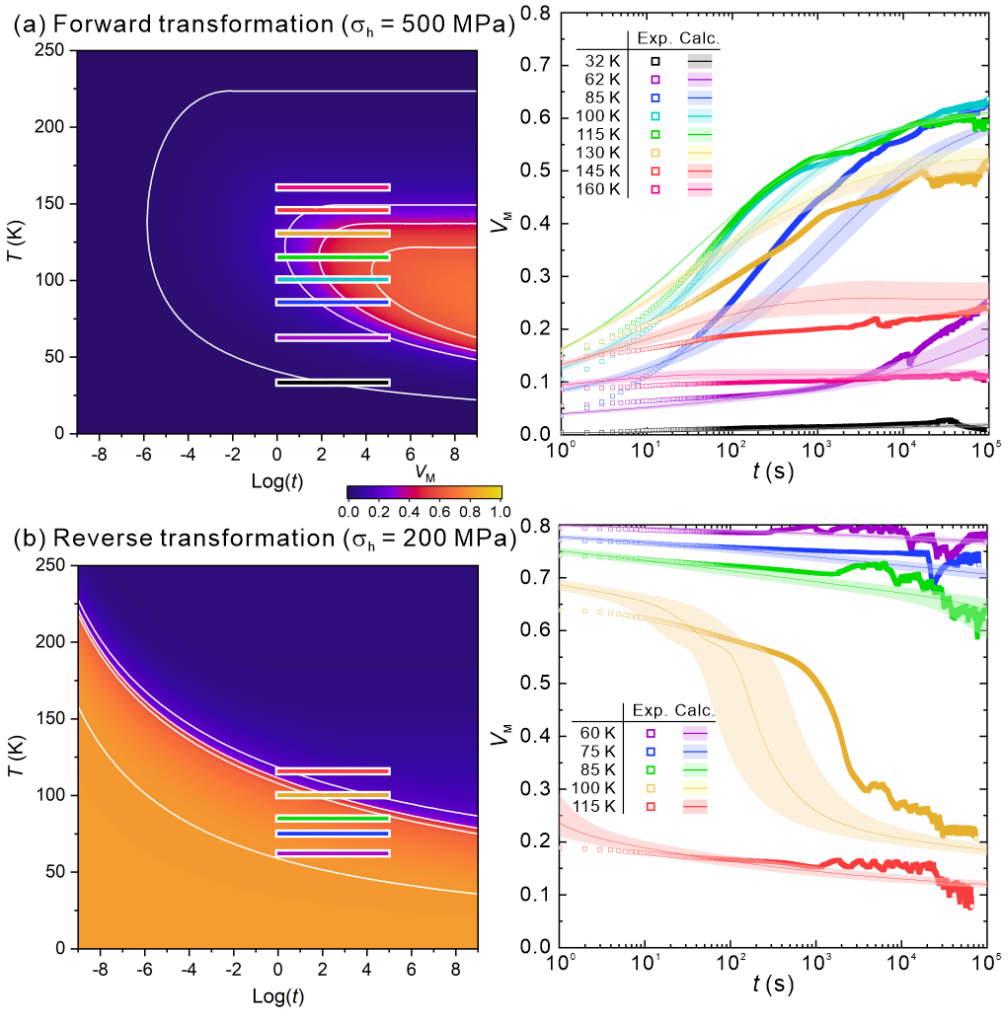

Fig. 6. Comparison of the calculated and experimental isothermal transformation dynamics for the (a) forward and (b) reverse transformation paths. The left panels show the calculated *TTT* diagrams at σ_h = (a) 500 and (b) 200 MPa, respectively. The right panels show the calculated and experimental variation in V_M as a function of time at several fixed temperatures. The masked regions reflect a temperature error of ±2 K in the calculations. Corresponding sections are overlaid onto their respective *TTT* diagrams with the same color.

3.3. IN-SITU OBSERVATION OF ISOTHERMAL GROWTH

The isothermal evolution of martensite was confirmed by *in situ* TEM observations under tensile stress. As soon as martensite nucleation was observed, dynamic elongation was interrupted and the isothermal growth under the holding

elongation was monitored. This observation was carried out at 220 and 95 K. The strain applied was estimated to be approximately 2.0% at 220 K and 0.8% at 95 K. Figure 7a and b presents time-series snapshots of several martensite variants nucleated near cleavages, respectively. The sketches of the evolution of the martensite edges (rightmost panels of Fig. 7a and b) show that the growth is remarkable at 95 K but stagnant at 220 K. The growth curve (Fig. 7c) captures the essential characteristics of the temperature dependence of the isothermal forward MT dynamics presented in Fig. 6a. It should be noted that the spatial stress distribution and magnitude are, of course, likely to be inhomogeneous with respect to location and time; therefore it is premature to discuss the detailed dynamics from these observations. However, they support that the remarkable temperature dependence of isothermal MT evolution shown in Fig. 6a is more or less attributable to the growth of martensite variants.

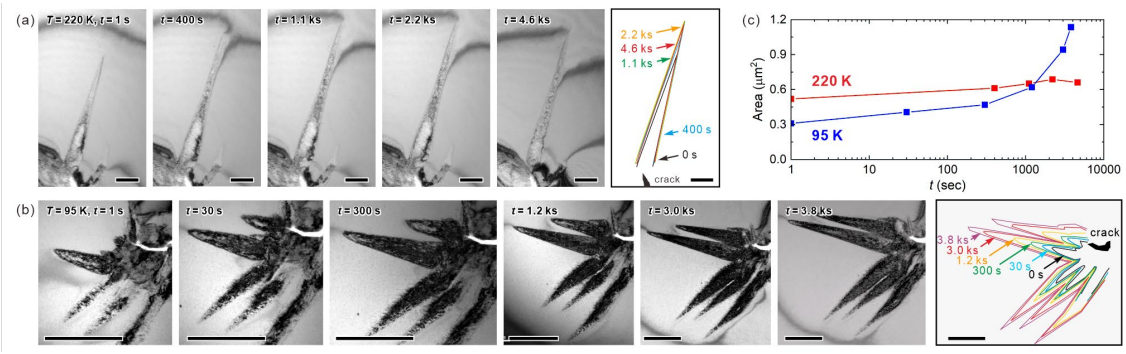

Fig. 7. Time-series snapshots of nucleated martensite variants at (a) 220 and (b) 95 K. The time scale was set from when the nucleation was confirmed. The evolution of the martensite edges over time is sketched in the rightmost figure of (a) and (b). (c) Changes in the area of a particular martensite variant over time. Scale bars, 500 nm.

3.4. TRANSFORMATION DYNAMICS UNDER COOLING/HEATING

The critical roles of thermal activation and thermodynamic equilibrium in the dynamics of isothermal MTs are explicitly visualized in the *TTT* diagrams. The *TTT* diagrams are convertible to continuous cooling/heating transformation (CCT/CHT) diagrams. The V_M change under continuous cooling can be derived by solving the path integral on the forward *TTT* diagrams, that is,

$$V_M(\mathbf{r}) = V_M(\mathbf{r}_0) + \int_{\mathbf{r}} \frac{\partial V_M(\mathbf{r})}{\partial t} dt + \Psi \int_{\mathbf{r}} \frac{\partial V_M(\mathbf{r})}{\partial T} dT$$

$$\text{where } \Psi = \begin{cases} -1 & (when\ \ \partial V_M(\mathbf{r})/\partial T < 0) \\ 0 & (when\ \ \partial V_M(\mathbf{r})/\partial T \geq 0) \end{cases} \qquad (4)$$

where $\mathbf{r} = (T, t)$ (in dimensionless units) represents the temperature sweep route. Let the starting point set $\mathbf{r}_0 = (250, 1)$ for the calculation of the CCT diagram. Whereas $\partial V_M / \partial t$ is always positive, $\partial V_M / \partial T$ becomes positive below the nose temperature, indicating the occurrence of the reverse MT. However, this case should not be involved in this path integral because the reverse MT is kinetically arrested in the low-temperature region; hence, Ψ is applied to $\int_{\mathbf{r}} \frac{\partial V_M(\mathbf{r})}{\partial T} dT$. The derivation of V_M change during the MT under continuous heating is analogous but somewhat complicated. Considering the calculation of the CHT diagram with a finite σ_h starting from $\mathbf{r}_0 = (0, 1)$ after zero-field (σ_h = 0) cooling (hereafter referred to as ZFC-FH), the V_M changes differently depending on the temperature range. When $T < T_\mu^M$ (T_μ^M is the temperature at which $\sigma_h = \sigma_0 + \sigma_\mu$), the following path integral is performed on the forward *TTT* diagrams:

$$V_M(\mathbf{r}) = V_M(\mathbf{r}_0) + \int_{\mathbf{r}} \frac{\partial V_M(\mathbf{r})}{\partial t} dt + \Psi' \int_{\mathbf{r}} \frac{\partial V_M(\mathbf{r})}{\partial T} dT$$

$$\text{where } \Psi' = \begin{cases} 1 & (when\ \ \partial V_M(\mathbf{r})/\partial T \geq 0) \\ 0 & (when\ \ \partial V_M(\mathbf{r})/\partial T < 0) \end{cases}. \qquad (5)$$

When $T_\mu^M \le T < T_\mu^A$ (T_μ^A is the temperature at which $\sigma_h = \sigma_0 - \sigma_\mu$), neither the forward nor reverse MTs proceeds, thus

$$\frac{\partial V_M(\mathbf{r})}{\partial t} = \frac{\partial V_M(\mathbf{r})}{\partial T} = 0 . \qquad (6)$$

Finally, the reverse MT progresses when $T_\mu^A \le T$. The following path integral is performed on the reverse *TTT* diagrams:

$$V_M(\mathbf{r}) = V_M(T_\mu^A, t_\mu^A) + \int_r \frac{\partial V_M(\mathbf{r})}{\partial t} dt + \Psi'' \int_r \frac{\partial V_M(\mathbf{r})}{\partial T} dT$$

$$\text{where } \Psi'' = \begin{cases} 1 & (when\ \partial V_M(\mathbf{r})/\partial T < 0) \\ 0 & (when\ \partial V_M(\mathbf{r})/\partial T \ge 0) \end{cases} . \qquad (7)$$

where t_μ^A represents the time at $T = T_\mu^A$. When V_M reaches 1 and 0, further forward and reverse MTs do not proceed, respectively. It is important to note that T_μ^M and T_μ^A are V_M-dependent.

Solving Eqs. 4, 5, 6, and 7 for various cooling/heating rates yields the CCT and CHT diagrams. Figure 8a and b shows representative CCT and CHT diagrams at $\sigma_h = 500$ MPa, respectively. These diagrams demonstrate that the MT dynamics are not simple, even under dynamic temperature sweep.

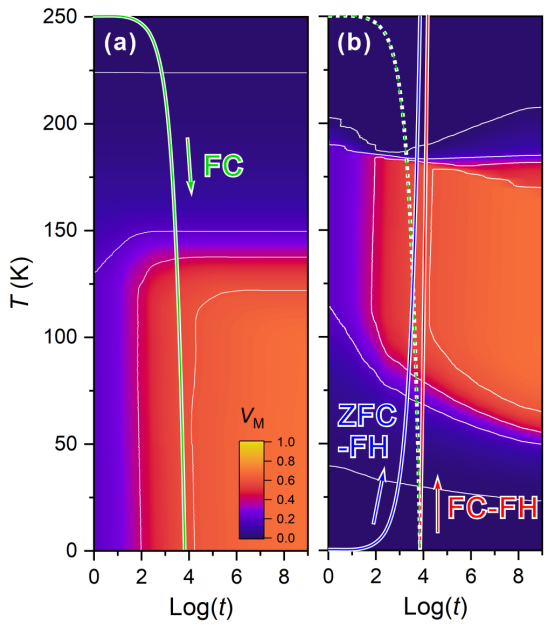

Fig. 8. (a) CCT and (b) CHT diagrams at σ_h = 500 MPa. The CHT diagram is derived for the ZFC-FH process. The overlaid lines are the temperature route defined in Fig. 10a.

4. DISCUSSION

4.1. MANIFESTATIONS OF THERMAL ACTIVATION

The isothermal *TTT* and dynamic CCT/CHT diagrams clarify the impact of time on both the isothermal and anisothermal MT dynamics. The findings will help interpret low-temperature MT dynamics, which are not comprehensively understood within the existing frameworks. More practically, elucidating the temperature sweep rate ($\dot{T}$) dependence of the forward MT starting/finishing temperatures (T_{Ms} and T_{Mf}) and the reverse MT starting/finishing temperatures (T_{As} and T_{Af}), is illustrative. Their $\dot{T}$ dependence can be derived from Fig. 4, as shown in Fig. 9a. These parameters exhibit a non-monotonic dependence on $\dot{T}$ as well as σ_h. This poses a fundamental concern that the commonly employed dynamic identifications of these parameters make sense only under the given conditions. T_{As} and T_{Af} moderately increase with increasing $\dot{T}$ and downshift with decreasing σ_h, and the transformation span (= $T_{Af} - T_{As}$) narrows with decreasing σ_h. In contrast, T_{Ms} and T_{Mf} exhibit a pronounced depression at a certain $\dot{T}$ range as can be observed at σ_h = 600 MPa for T_{Mf}, and σ_h = 400 MPa for T_{Ms}. At σ_h = 0 and 300 MPa, T_{Ms} and T_{Mf} can no longer be defined within the temperature window shown. A similar $\dot{T}$ dependence has been reported in a Ti-50.2Ni alloy (see the lowest panel of Fig. 9a), although resolving the subtle difference in their $\dot{T}$ dependencies is difficult [43]. Following the basic concept of Eq. 1, the characteristic temperatures (T_{Ms}, T_{Mf}, T_{As}, and

T_{Af}) can be decomposed into the $\dot{T}$-independent athermal and $\dot{T}$-dependent thermal terms. The latter term is difficult to capture at elevated temperatures where the thermal excitations occur very quickly; therefore, the measured values are less dependent on $\dot{T}$. This term can be captured at lower temperatures (typically below 200 K). This situation allows for isothermal MT to drive even above the experimentally determined T_{Ms}, as has been reported to occur [2,44].

The $\dot{T}$ dependence of T_{Ms} and T_{Mf} is particularly noteworthy as their pronounced depression means that the occurrence of kinetic arrest is controllable by changing $\dot{T}$ and σ_h. The cooling rate dependence of the volume of the kinetically arrested austenite phase $(1 - V_M)$ is an informative and experimentally tractable measure. As shown in Fig. 9b, V_M at 0 K, as estimated from Fig. 8a for σ_h = 500 MPa, exhibits a non-monotonic dependence on the cooling rate. Indeed, a similar cooling rate dependence has been experimentally observed in a different type of 1st-order transformation with a similar temperature dependence of the transformation hysteresis [45]. The kinetic arrest can also be observed in magnetic-field-induced MT systems [46]. The same principle holds analogously when magnetic fields or chemical driving forces are applied.

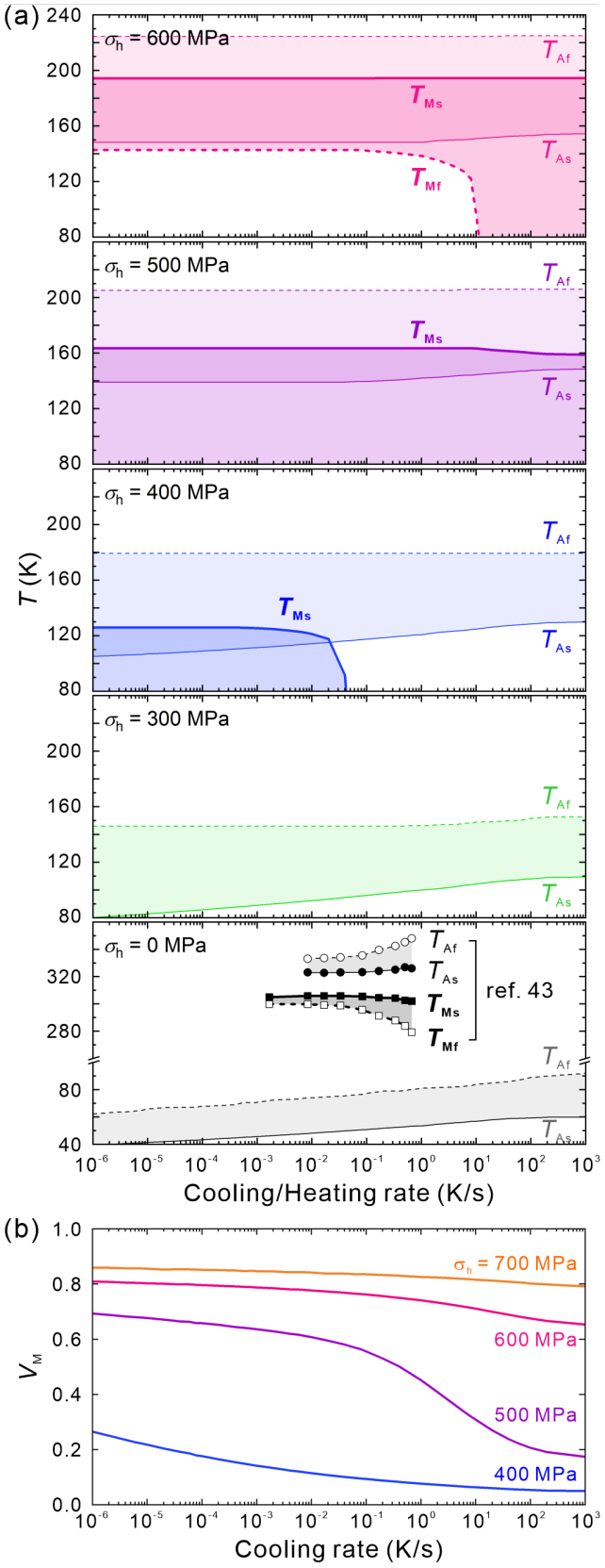

Fig. 9. (a) Temperature sweep rate dependence of T_{Ms}, T_{Mf}, T_{As}, and T_{Af} at various σ_h, where T_{Ms}/T_{Af} are defined as the temperatures at which $V_M = 0.1$ upon cooling/heating and T_{Mf}/T_{As} are defined as the temperatures at which $V_M = 0.7$ upon cooling/heating, respectively. The plot in the lowest panel was obtained from ref. [43]. Masked regions

indicate the transformation spans of $T_{Ms} - T_{Mf}$ and $T_{Af} - T_{As}$. (b) Cooling rate dependence of V_M at 0 K at various σ_h.

4.2. INTERPRETATION OF NON-ERGODICITY

The glass-like thermal history dependence of strain is referred to as non-ergodicity and is believed to be an essential signature of strain glass [36,37]. In light of the concept of viscosuperelasticity, the thermal history dependence of V_M can be discussed based on the derived CCT and CHT diagrams. As an example, the changes in V_M were calculated via Eqs. 4, 5, 6, and 7 for the following three cooling/heating routes overlaid in Fig. 8a and b, namely, at a cooling rate of 0.04 K/s with σ_h = 500 MPa (FC); at a heating rate of 0.04 K/s with σ_h = 500 MPa after FC (FC-FH); and at a heating rate of 0.04 K/s with σ_h = 500 MPa after quenching to 0 K without stress (ZFC-FH). The results are presented in Fig. 10a as a function of temperature. The thermal history dependence of V_M is evidence that the observed MT dynamics are not ergodic. In the ZFC-FH curve, V_M initially increases in response to the heating-induced forward MT, reaches a stable value between T_μ^M and T_μ^A, and then converges to zero due to the reverse MT upon further heating. A similar trend is observed in the FC-FH curve, but the initial increase is less significant because the forward MT is largely completed during the FC process. For reference, the hypothetical ZFC-FH and FC-FH curves assuming $T_\mu^A = T_\mu^M$ (that is, without hysteresis) are shown by the dotted lines in Fig. 10a. The hypothetical ZFC-FH curve, in comparison to the actual case, exhibits a narrower peak near the nose temperature and exhibits very little thermal history dependence above this temperature.

Additionally, the hypothetical FC-FH curve exhibits high reproducibility with the FC curve. These trends mimic the typical non-ergodic behavior in spin glass and relaxor systems [47,48]. However, such a feature would not be observed in MTs because the transformation hysteresis must exist. The contrasting behavior of the modeled (filled lines) and hypothetical (dotted lines) cases shows that the origin of non-ergodic strains can be inferred from the observed thermal history dependence. A broader hump in the ZFC-FH curve and the apparent history dependence above the nose temperature manifest the activation of MTs rather than what would be expected in the strain glass state.

Figure 10b and c presents examples with a significantly lower σ_h together with reference data [36,49]. The difference between the experimental and calculated curves, especially the sharpness of the reverse MT, deserves additional remarks. Small σ_h corresponds to a small V_M and results in a faint difference between the reverse transformation starting/finishing temperatures (This tendency can be seen in Fig. 9a). Since the calculation does not account for microstructural and chemical heterogeneities, the transformation dynamics are specified to proceed uniformly along the CCT/CHT diagrams. However, in reality, microstructural and chemical heterogeneities locally disturb the transformation temperatures. Besides, the elastocaloric cooling effect may widen the reverse MT span. The ZFC-FH curves of refs. 36 and 49 start to decrease at a temperature apparently higher than the nose temperature. This trend was reproduced in our model, supporting the activation of MTs. Indeed, a small amount of martensite is inducible even under such small stresses, as reported in ref. 50. Such martensite could

presumably breathe in the vicinity of stress-concentrated regions, such as cracks, grain boundaries, precipitates, and surfaces, contributing to the non-ergodic response. Additionally, it is important to mention another possibility that could mislead to the branding of strain glass. Another type of MT, called the R-phase transformation, may be stress-induced at the temperature and stress condition where the B2-B19' MT is kinetically arrested [30]. The R-phase transformation accompanies an exceptionally narrow temperature hysteresis and small transformation strain [51,52]. Once this transformation takes place, it could be difficult to discern the signature of hysteretic MTs in the thermal history dependence of V_M.

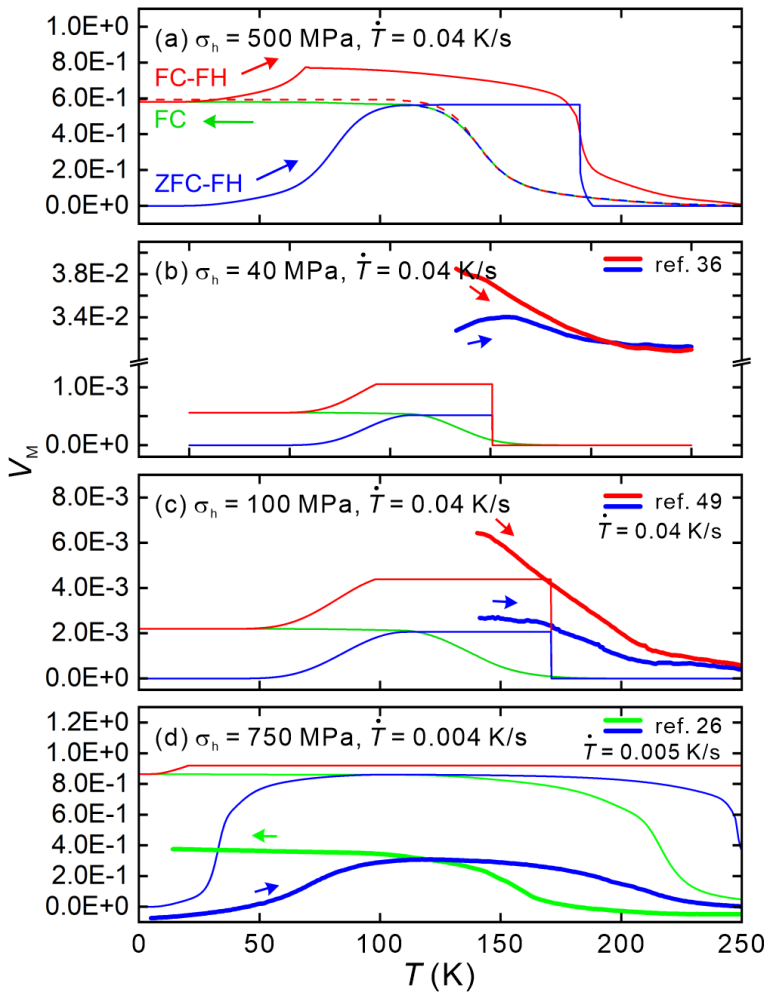

Fig. 10. The variation in V_M change in the FC, FC-FH, and ZFC-FH routes overlaid in Fig. 8a and b: (a) σ_h = 500 MPa and $\dot{T}$ = 0.04 K/s, (b) σ_h = 40 MPa and $\dot{T}$ = 0.04 K/s,

(c) σ_h = 100 MPa and $\dot{T}$ = 0.04 K/s, and (d) σ_h = 750 MPa and $\dot{T}$ = 0.004 K/s. The ZFC-FH and FC-FH curves assuming $T_\mu^A = T_\mu^M$ are shown together in (a) with broken lines. The reference data with a comparable $\dot{T}$ is shown together in (b), (c), and (d) [26,36,49]. Here, the reference data were originally given in strain and were converted to V_M by dividing by ε_{full} after subtracting the elastic strain referring to the temperature dependence of E_A given in ref. 49. Note that $\dot{T}$ was not addressed in ref. 36. Vertical mismatch in V_M could be attributed to compositional difference or inaccuracy in measured strain or E_A.

More apparent signatures of the thermal activation of MTs can be captured at a larger σ_h, as shown in Fig. 10d. A broad peak in the ZFC-FH curve and a remarkable history dependence above the nose temperature can be observed experimentally [26]. This behavior has also been observed in the magnetic-field-induced MT of a Ni-Co-Mn-In alloy [53].

Kustov also discussed the origin of non-ergodic strain from a different perspective to that of strain glass, stating that a large part of the strain observed in the so-called strain glass state is elastic strain, and claiming that the remaining non-ergodic component (in the order of 10^{-3} in V_M) originates from the precursor martensitic nanodomains [49]. However, the detailed reason for the non-ergodic behavior attributed to such nanodomains has yet to be explicitly addressed. The findings in the present study strongly suggest that this non-ergodic behavior originates from the thermal activation of martensite growth rather than the glassy strain state of the austenite phase. This conclusion raises a concern about the unique branding between strain glass and non-ergodicity. Apart from the universality of the concept of strain glass, the non-ergodic

behavior of V_M can be interpreted as a manifestation of the isothermal propagations of habit planes, which is now predicated upon the concept of viscosuperelasticity.

4.3. SIGNIFICANCE OF THERMAL ACTIVATION

Following a number of studies on the dynamics of thermoelastic MTs, three different claims on the athermal/isothermal nature have been made. Firstly, two distinct types of athermal and isothermal dynamics exist depending on the alloy system, temperature, and/or directions of the MTs [1,2,4,16–18,42]. Secondly, thermal activation exists to a greater or lesser extent in all thermoelastic MT systems [25,54–57]. Lastly, MTs are always athermal due to their diffusionless/displacive nature [58,59]. The isothermal experimental results in this study (see Figs. 5 and 6) reveal that the isothermal MT proceeds even at 62 K, where atomic diffusion is unlikely to occur, thus negating the possibility of the third claim. Furthermore, as previously claimed by Kajiwara [19–21], the propagation of martensite variants is accompanied by dislocation motion. This claim supports the isothermal growth of MT without the need for atomic diffusion and, more importantly, envisages the validity of our thermal activation model mimicking the classical thermal activation theory for dislocation glides. Kustov [42] performed similar experiments on this alloy system and classified the three transformation paths of B2-B19', B2-R-B19', and B2-B19-B19' as either athermal or isothermal. He therein concluded that the forward B2-B19' transformation is isothermal but the reverse B19'-B2 transformation is likely athermal, and therefore claimed that the athermal/isothermal distinction is

attributable to a distinction in strain accommodation, inferred from the difference of thermal hysteresis in relation to the types of MTs. However, this conclusion was drawn based on experiments above 180 K, where the isothermal nature is difficult to capture, and as demonstrated in Fig. 9a, the temperature hysteresis varies with the temperature sweep rate; therefore, it cannot be a unique scale for comparison. In a Cu-Al-Ni system, Kakeshita detected isothermal incubation of the reverse MT. He discussed this in the same way as isothermal incubation of the forward MT based on his nucleation model [55]. However, it is questionable whether the underlying concept of "nucleation" can be applied to the reverse MT and even to the growth process. Like other existing models, Kakeshita's approach does not account for the role of thermodynamic equilibrium; therefore, there is no way to describe the non-reciprocity in the forward and reverse MT dynamics. Nevertheless, although based on the nucleation concept, Kakeshita's approach leads to an interpretation that integrates athermal and isothermal dynamics [54,56,57], proposing a sequential schema bridging athermal and isothermal in the *TTT* diagram for the forward MT. The results in this study basically support his interpretation (that is, the second claim) and quantitatively consolidate it in terms of the growth dynamics with accounting for the thermodynamic equilibrium boundary that forms a spine in the phase diagram.

Almost all existing studies have tackled isothermal dynamics by changing only the isothermal holding temperature. However, this approach is most likely to overlook the impact of thermal activation on the reverse MT because, as shown in Fig. 9a, the shifts

of T_{As} and T_{Af} are less visible in most cases. Based on our phase diagram shown in Figs. 1b and 3, the significance of thermal activation should be assessed by screening external variables, such as stresses and magnetic fields (and also chemical composition), in addition to temperature.

The most straightforward measure of the significance of thermal activation is σ_{TA}. As shown in Fig. 11, σ_{TA} differs by more than 3 orders among the studied alloy systems [27,60–62]. Kustov assumes that the difference should be primarily related to the distinction in strain accommodation [42]. Yet, even accounting for various effects arising from crystallographic differences, σ_{TA} in a Ti-Ni system is anomalously large. The origin of this anomaly remains an open question. The authors assume that the precursor commensurate/incommensurate nanodomains [63,64] or the intermartensitic R-phase [51] may be crucial in amplifying σ_{TA} in this system. This perspective will be discussed in the near future.

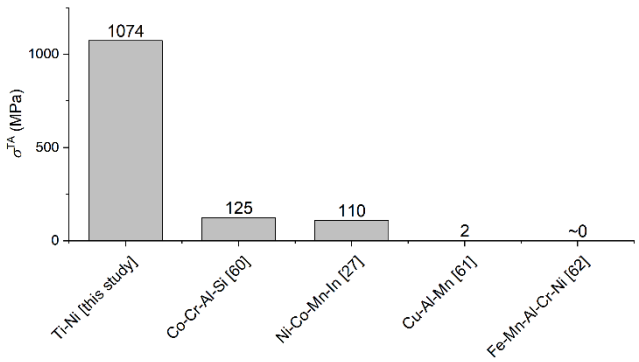

Fig. 11. Comparison of σ_{TA} for the studied systems [27,60–62].

5. CONCLUSIONS

This study presents a new approach for clarifying the impact of thermal activation upon MT evolutions, typically manifested below room temperature. The thermal activation component of transformation hysteresis is shown to vary with time and temperature. The isothermal *TTT* diagrams for the forward and reverse MTs are non-reciprocal. The *TTT* diagrams for the forward MT show typical C-shaped contour curves, whereas those for the reverse MT show the lower half of the C-shaped contour curves. The *TTT* diagrams are further converted to the CCT/CHT diagrams. These diagrams explain that the sweep rate dependence of the characteristic temperatures (T_{Ms}, T_{Mf}, T_{As}, and T_{Af}) and the non-ergodic thermal-history dependence of anelastic transformation strain are ascribed to the thermally activated sluggish MT dynamics. This raises a concern about the unique branding between non-ergodicity and the concept of strain glass.

The proposed scheme offers a unified picture of the dynamics of thermoelastic MTs involving the impacts of athermal and isothermal dynamics. Since the underlying framework is an extension of the thermal activation model of plastic deformation, it sheds light on the similarities between the thermally activated sluggish dynamics of habit plane propagations and dislocation glides. A new concept of "viscosuperelasticity" is introduced following the concept of viscoplasticity. This concept provides a straightforward interpretation; kinetic arrest and strain glass, which were thought to be distinct and unrelated phenomena, are to be interpreted as having the same roots of "viscosuperelastic" dynamics. This concept allows a more comprehensive understanding of various manifestations related to the thermal activation of MTs

1

Data availability

The raw data related to this manuscript will be made available upon reasonable request.

Declaration of Competing Interest

The authors declare that they have no known competing financial interests or personal relationships that could have appeared to influence the work reported in this paper.

Acknowledgments

The authors acknowledge fruitful discussions with K. Matsuura and H. Oike. This study was supported by the Mizuho Foundation for the Promotion of Sciences, Kyoto University Foundation, JST PRESTO (Grant Number JPMJPR22Q6), and JSPS KAKENHI (Grant Numbers 19H02418 and 19K22052).

Appendix

A. Mathematical fitting of the superelastic stress-strain curves

V_M was estimated from the stress-strain curves to analyze the isothermal evolutions of martensite. A mathematical fitting was performed on the dynamic superelastic stress-strain curves to estimate V_M as a function of stress. Representative examples of fittings are shown in Fig. A1a and b for the stress-strain curves at 115 and 100 K exhibiting the dynamic forward and reverse MTs, respectively. Based on the

existing constitutive equations [65,66], this study employed the following equation for fitting:

$$\sigma = E_{mix}\varepsilon + \Omega V_M \qquad \text{(A.1)}$$

where E_{mix} is the effective elastic modulus as a function of V_{M} and Ω is the transformation coefficient; they are given by $E_{mix} = E_A + V_M\left(E_M - E_A\right)$ and $\Omega = -\varepsilon_{SE}E_{mix}$, respectively. The elastic moduli of austenite and martensite (E_{A} and E_{M}, respectively) were estimated by least-squares fitting to be 17.5 and 18.2 GPa, respectively, at 100 K and 16.6 GPa and 17.6 GPa, respectively, at 115 K. Note that these values are considerably lower than the reported values [67] because they include the elastic modulus of the compression jig inside the cooling chamber. The following asymmetric sigmoid function [68] was employed to fit the evolution of V_{M}:

$$V_M = B + \frac{A - B}{\left\{1 + \upsilon \exp\left[-\lambda(\varepsilon - \varepsilon_c)\right]\right\}^{1/\upsilon}} \qquad \text{(A.2)}$$

where A and B are the upper and lower limits, respectively, λ is a shape parameter, υ is a parameter characterizing the asymmetric curvature, and ε_{c} is the inflection point. The resultant fitting curves (Fig. A1a and b) accurately trace the experimental curves with the evolution of V_{M} (Fig. A1c and d) as estimated using Eq. A.2. Furthermore, polynomial fitting was employed to convert the evolution of V_{M} into a function of stress (Fig. A1e).

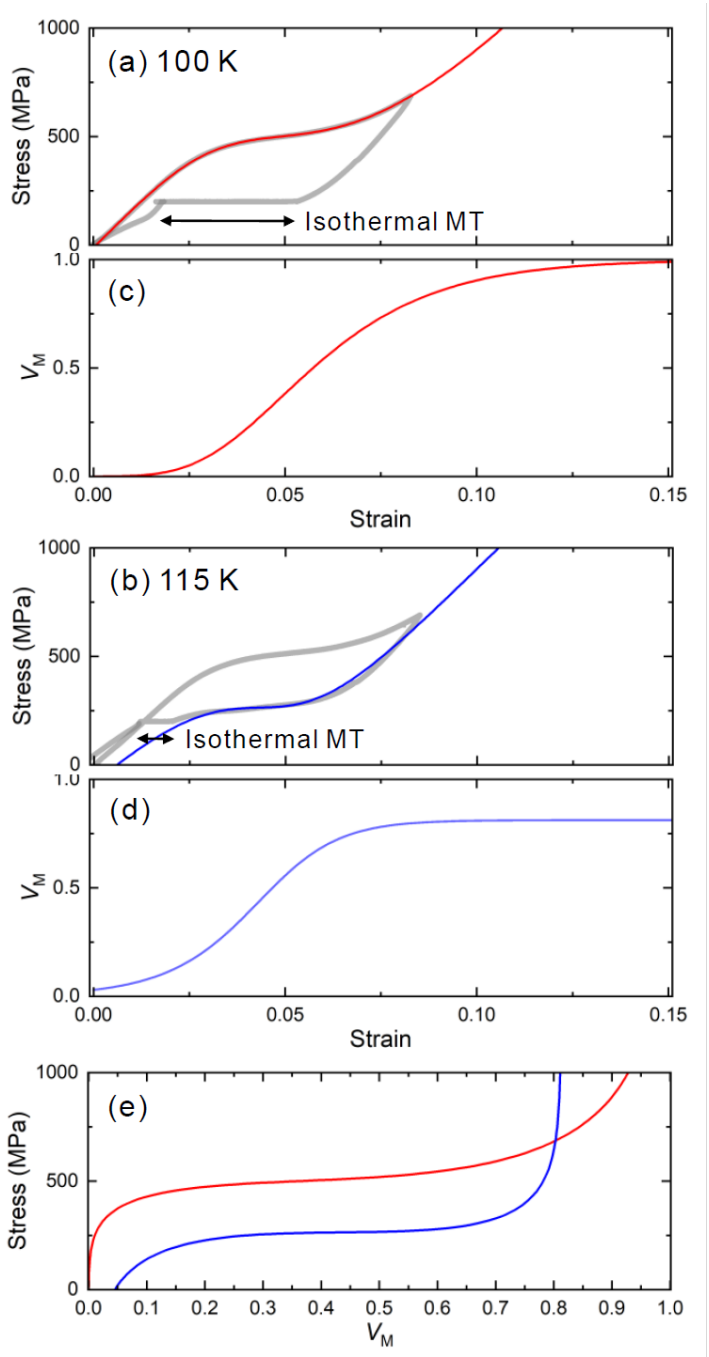

Fig. A1. Stress–strain curves at (a) 100 and (b) 115 K; gray and colored curves represent the experimental and fitted data, respectively. Evolution of V_M at (c) 100 and (d) 115 K as a function of strain and (e) as a function of stress. The numerical values of the parameters in Eq. (B.2) are as follows: $A = 1$ (at 100 K) and 0.81 (at 115 K), $B = 0$ (at 100 and 115 K), $\lambda = 45.0$ (at 100 K) and 100.8 (at 115 K), $\upsilon = 1.0 \times 10^{-9}$ (at 100 K) and 1.4 (at 115 K), $\varepsilon_c = 0.049$ (at 100 K) and 0.043 (at 115 K).

References

[1] G. V. Kurdjumov, O. P. Maksimova, Kinetics of Austenite-To-Martensite Transformation at Low Temperatures, Dokl. Akad. Nauk SSSR 61 (1948) 83-86.

[2] G. V. Kurdjumov, O. P. Maksimova, Work Required in the Formation of Martensite Nuclei, Dokl. Akad. Nauk SSSR 73 (1950) 95-99

[3] E. S. Machlin, M. Cohen, Isothermal Mode of the Martensitic Transformation, Trans. Metall. Soc. AIME 194 (1952) 489-500.

[4] R. E. Cech, J. H. Hollomon, Rate of Formation of Isothermal Martensite in Fe-Ni-Mn, Trans. Metall. Soc. AIME 197 (1953) 685-691.

[5] J. C. Fisher, Application of Nucleation Theory to Isothermal Martensite, Acta Metall. 1 (1953) 32-35.

[6] C. H. Shih, B. L. Averbach, M. Cohen, Some Characteristics of the Isothermal Martensitic Transformation, Trans. Metall. Soc. AIME 203 (1955) 183-187.

[7] V. Raghavan, Martensite, ASM International, Materials Park, Ohio, 1992.

[8] T. Fukuda, T. Kakeshita, Y. H. Lee, An interpretation of the kinetics of martensitic transformation in a $Ni_{45}Co_5Mn_{36.5}In_{13.5}$ alloy, Acta Mater. 81 (2014) 121-127.

[9] F. J. Romero, J. Manchado, J. M. Martín-Olalla, M. C. Gallardo, E. K. H. Salje, Dynamic heat flux experiments in $Cu_{67.64}Zn_{16.71}Al_{15.65}$: Separating the time scales of fast and ultra-slow kinetic processes in martensitic transformations, Appl. Phys. Lett. 99 (2011) 011906.

[10] H. Kato, R. Stalmans, J. Van Humbeeck. Two-Way Shape Memory Effect Induced

by Tension Training in Cu-13.4Al-4.0Ni (mass%) Alloy Single Crystals, Mater. Trans. 39 (1998) 378-386.

[11] G. Ghosh, V. Raghavan, The kinetics of isothermal martensitic transformation in an Fe-23.2wt.%Ni-2.8wt.%Mn alloy, Mat. Sci. Eng. A 80 (1986) 65-74.

[12] L. Kaufman, M. Cohen, Thermodynamics and kinetics of martensitic transformations, Progr. Metal Phys. 7 (1958) 165-246.

[13] V. Raghavan, M. Cohen, A nucleation model for martensitic transformations in iron-base alloys, Acta Metall. 20 (1972) 333-338.

[14] G. B. Olson, M. Cohen, A general mechanism of martensitic nucleation: Part I. General concepts and the FCC→ HCP transformation, Met. Trans. 7A (1976) 1897-1904.

[15] G. B. Olson, M. Cohen, A general mechanism of martensitic nucleation: Part II. FCC → BCC and other martensitic transformations, Met. Trans. 7A (1976) 1905-1914.

[16] G. B. Olson, M. Cohen, A General Mechanism of Martensitic Nucleation: Part III. Kinetics of Martensitic Nucleation, Met. Trans. 7A (1976) 1915-1923.

[17] G. Ghosh, G. B. Olson, Kinetics of FCC → BCC heterogeneous martensitic nucleation−I. The critical driving force for athermal nucleation, Acta Metall. Mater. 42 (1994) 3361-3370.

[18] G. Ghosh, G. B. Olson, Kinetics of F.c.c. → b.c.c. heterogeneous martensitic nucleation−II. Thermal activation, Acta Metall. Mater. 42 (1994) 3371-3379.

[19] S. Kajiwara, Morphology and crystallography of the isothermal martensite

transformation in Fe—Ni—Mn alloys, Philos. Mag. 43 (1981) 1483-1503

[20] S. Kajiwara, EFFECT OF APPLIED STRESS ON NUCLEATION RATE OF ISOTHERMAL MARTENSITIC TRANSFORMATION, J. Phys. Colloques 43 (1982) C4-97-102

[21] T. Kikuchi, S. Kajiwara, HVEM in situ observation of isothermal martensitic transformation under applied stress, Trans. Japan Inst. Metals 26 (1985) 861-868.

[22] L. Carrillo, J. Ortín, Avalanches in the growth of stress-induced martensites, Phys. Rev. B 56 (1997) 11508.

[23] V. Raghavan, A. R. Entwisle, Physical properties of martensite and bainite, Technical Report Special Report No. 93, Iron and Steel Institute, London, 1965.

[24] S. R. Pati, M. Cohen, Kinetics of isothermal martensitic transformations in an iron-nickel-manganese alloy, Acta Metall. 19 (1971) 1327-1332

[25] T. Kakeshita, K. Kuroiwa, K. Shimizu, T. Ikeda, A. Yamagishi, M. Date, A New Model Explainable for Both the Athermal and Isothermal Natures of Martensitic Transformations in Fe–Ni–Mn Alloys, Mater. Trans. JIM 34 (1993) 423-428.

[26] K. Niitsu, T. Omori, R. Kainuma, Stress-induced transformation behaviors at low temperatures in Ti-51.8 Ni (at.%) shape memory alloy, Appl. Phys. Lett. 102 (2013) 231915.

[27] K. Niitsu, X. Xu, R. Y. Umetsu, R. Kainuma. Stress-induced transformations at low temperatures in a $Ni_{45}Co_5Mn_{36}In_{14}$ metamagnetic shape memory alloy, Appl. Phys. Lett. 103 (2013) 242406.

[28] K. Niitsu, R. Kainuma, Effect of annealing on stress-induced transformation behaviors at low temperatures in a Ti‑51.8 at.% Ni shape memory alloy, Phys. Stat. Sol. (b) 251 (2014) 2041-2047

[29] Y. Kimura, X. Xu, K. Niitsu, T. Omori, R. Kainuma, Martensitic transformations and superelastic behavior at low temperatures in Ti50− xNi40+ xCu10 shape memory alloys, Mater. Trans. 57 (2016) 269-277.

[30] K. Niitsu, Y. Kimura, R. Kainuma, Transformation entropy change and precursor phenomena in Ni-rich Ti–Ni shape memory alloys, J. Mater. Res. 32 (2017) 3822-3830.

[31] K. Niitsu, H. Date, R. Kainuma, Thermal activation of stress-induced martensitic transformation in Ni-rich Ti-Ni alloys, Scr. Mater. 186 (2020) 263-267.

[32] T. Odaira, S. Xu, X. Xu, T. Omori, R. Kainuma, Elastocaloric switching effect induced by reentrant martensitic transformation, Appl. Phys. Rev. 7 (2020) 031406.

[33] A. Seeger, The temperature dependence of the critical shear stress and of work-hardening of metal crystals, Philos. Mag. 45 (1954) 771-773.

[34] U. F. Kocks, A. S. Argon, M. F. Ashby, Progress in Materials Science, in: B. Chalmers, J. W. Christian, T. B. Massalski (Eds.), 19, Pergamon Press, Oxford, 1975.

[35] H. Mecking, U. F. Kocks, Kinetics of flow and strain-hardening, Acta Metall. 29 (1981) 1865-1875.

[36] Y. Wang, X. Ren, K. Otsuka, A. Saxena, Evidence for broken ergodicity in strain glass, Phys. Rev. B 76 (2007) 132201.

[37] X. Ren, Y. Wang, Y. Zhou, Z. Zhang, D. Wang, G. Fan, K. Otsuka, T. Suzuki, Y. Ji, J. Zhang, Y. Tian, S. Hou, X. Ding, Strain glass in ferroelastic systems: Premartensitic tweed versus strain glass, Philos. Mag. 90 (2010) 141-157.

[38] https://www.gatan.com/products/tem-specimen-holders/straining-situ-holders

[39] H. C. Tong, C. M. Wayman, Characteristic temperatures and other properties of thermoelastic martensites, Acta Metall. 22 (1974) 887-896.

[40] K. Niitsu, Y. Kimura, X. Xu, R. Kainuma, Composition dependences of entropy change and transformation temperatures in Ni-rich Ti–Ni system, Shap. Mem. Superelasticity. 1 (2015) 124-131.

[41] D. François, A. Pineau, A. Zaoui, Mechanical Behaviour of Materials Volume II: Viscoplasticity, Damage, Fracture and Contact Mechanics, Kluwer Academic Publishers (1993).

[42] S. Kustov, D. Salas, E. Cesari, R. Santamarta, J. Van Humbeeck, Isothermal and athermal martensitic transformations in Ni–Ti shape memory alloys, Acta Mater. 60 (2012) 2578-2592.

[43] Q. Meng, H. Yang, Y. Liu, T. Nam, Transformation intervals and elastic strain energies of B2-B19’ martensitic transformation of NiTi, Intermetallics 18 (2010) 2431-2434

[44] S. A. Kulin, G. R. Speich, Isothermal Martensite Formation in an Iron-Chromium-Nickel Alloy, Trans. Am. Inst. Mining Metall. Eng. 194 (1952) 258-263.

[45] K. Matsuura, H. Oike, V. Kocsis, T. Sato, Y. Tomioka, Y. Kaneko, M. Nakamura,

Y. Taguchi, M. Kawasaki, Y. Tokura, F. Kagawa, Kinetic pathway facilitated by a phase competition to achieve a metastable electronic phase, Phys. Rev. B 103 (2021) L041106.

[46] W. Ito, K. Ito, R. Y. Umetsu, R. Kainuma, Kinetic arrest of martensitic transformation in the NiCoMnIn metamagnetic shape memory alloy, Appl. Phys. Lett. 92 (2008) 021908.

[47] J. A. Mydosh, Spin glasses: an experimental introduction, Taylor & Francis, London, 1993.

[48] R. A. Cowley, S. N. Gvasaliya, S. G. Lushnikov, B. Roessli, G. M. Rotaru, Relaxing with relaxors: a review of relaxor ferroelectrics, Adv. Phys. 60 (2011) 229-327.

[49] S. Kustov, D. Salas, E. Cesari, R. Santamarta, D. Mari, J. Van Humbeeck, Structural anelasticity, elasticity and broken ergodicity in Ni–Ti shape memory alloys, Acta Mater. 73 (2014) 275-286.

[50] G. F. Nataf, M. Romanini, E. Vives, B. Žužek, A. Planes, J. Tušek, X. Moya, Suppression of acoustic emission during superelastic tensile cycling of polycrystalline $Ni_{50.4}Ti_{49.6}$, Phys. Rev. Materials 4 (2020) 093604.

[51] X. B. Wang, B. Verlinden, J. Van Humbeeck, R-phase transformation in NiTi alloys, Mat. Sci. Technol. 30 (2014) 1517-1529.

[52] T. W. Duerig, K. Bhattacharya, The Influence of the R-Phase on the Superelastic Behavior of NiTi, Shap. Mem. Superelasticity, 1 (2015) 153-161.

[53] Y.-H. Lee, M. Todai, T. Okuyama, T. Fukuda, T. Kakeshita, R. Kainuma, Isothermal

nature of martensitic transformation in an $Ni_{45}Co_5Mn_{36.5}In_{13.5}$ magnetic shape memory alloy, Scr. Mater. 64 (2011) 927-930.

[54] T. Kakeshita, K. Kuroiwa, K. Shimizu, T. Ikeda, A. Yamagishi, M. Date, Effect of Magnetic Fields on Athermal and Isothermal Martensitic Transformations in Fe–Ni–Mn Alloys, Mater. Trans. JIM 34 (1993) 415-422.

[55] T. Kakeshita, T. Takeguchi, T. Fukuda, T. Saburi, Time-Dependent Nature of the Athermal Martensitic Transformation in a Cu–Al–Ni Shape Memory Alloy, Mater. Trans. JIM 37 (1996) 299-303.

[56] T. Kakeshita, J.-M. Nam, T. Fukuda, Kinetics of martensitic transformations in magnetic field or under hydrostatic pressure, Sci. Tech. Adv. Mater. 12 (2011) 015004.

[57] T. Fukuda, T. Kakeshita, Y.-H. Lee, An interpretation of the kinetics of martensitic transformation in a $Ni_{45}Co_5Mn_{36.5}In_{13.5}$ alloy, Acta Mater. 81 (2014) 121-127.

[58] M. Kozuma, Y. Murakami, T. Kawano, K. Otsuka, An isothermal martensitic transformation in a quenched Au-49.5at%Cd alloy, Scr. Mater. 36 (1997) 253-258.

[59] K. Otsuka, X. Ren, T. Takeda, Experimental test for a possible isothermal martensitic transformation in a Ti–Ni alloy, Scr. Mater. 45 (2001) 145-152.

[60] T. Odaira, S. Xu, X. Xu, T. Omori, R. Kainuma, Elastocaloric switching effect induced by reentrant martensitic transformation, Appl. Phys. Rev. 7 (2020) 031406.

[61] K. Niitsu, Y. Kimura, T. Omori, R. Kainuma, Cryogenic superelasticity with large elastocaloric effect, NPG Asia Mater. 10 (2018) e457.

[62] J. Xia, Y. Noguchi, X. Xu, T. Odaira, Y. Kimura, M. Nagasako, T. Omori, R. Kainuma, Iron-based superelastic alloys with near-constant critical stress temperature dependence, Science 369 (2020) 855-858.

[63] C. M. Hwang, M. Meichle, M. B. Salamon, C. M. Wayman, Transformation behaviour of a Ti50Ni47Fe3 alloy I. Premartensitic phenomena and the incommensurate phase, Philos. Mag. A 47 (1983) 9-30.

[64] Y. Murakami, H. Shibuya, D. Shindo, Precursor effects of martensitic transformations in Ti-based alloys studied by electron microscopy with energy filtering, J. Microsc. 203 (2001) 22-33.

[65] K. Tanaka, A Thermomechanical Sketch of Shape Memory Effect: One-dimensional Tensile Behavior, Res. Mechanica 18 (1986) 251.

[66] Y. G. Zhu, H. X. Lu, D. Z. Yang, A New Model of Shape Memory Alloys, Appl. Math. Mech. 23 (2002) 896.

[67] T. Mita, K. Kawashima, M. Misumi, M. Ohkubo, Poisson's Ratio and Young's Modulus of TiNi Shape Memory Alloy Measured by Electromagnetic Acoustic Transducer, Trans. Jap. Soc. Mech. Eng. A 76 (2010) 290-295.

[68] F. J. Richards, A Flexible Growth Function for Empirical Use, J. Exp. Bot. 10 (1959) 290-301.